(25) U. Schindewolf, *Angew. Chem. Int' Ed Engl.*, **7**, 190 (1968).
(26) S. Naiditch, O. A. Paez and J. C. Thompson, *J. Chem. Eng. Data*, **12**, 164 (1967).
(27) C. A. Kraus, E. S. Carney and W. C. Johnson, *J. Amer. Chem. Soc.*, **49**, 2206 (1927).
(28) U. Schindewolf and M. Werner, *J. Phys. Chem.*, **84**, 1123 (1980).
(29) H. Eyring, *J. Chem. Phys.*, **4**, 283 (1936).
(30) W. J. Moore, "Physical Chemistry", 4th Ed., p. 921, Prentice–Hall, Englewood Cliffs, N. J., 1959.
(31) T. Nozaki and M. Shimoji, *Trans. Faraday Soc.*, **65**, 1489 (1969).
(32) K. W. Böddeker, G. Lang and U. Schindewolf, in ref. 19.

Molecular Theory of Plastic Deformation (III)*

Jae Hyun Kim and Taikyue Ree†

Department of Chemistry, Korea Advanced Institute of Science and Technology, P. O. Box 150 Chongyangni, Seoul 131, Korea

Chang Hong Kim

Analytical Chemistry Laboratory, Korea Advanced Institute of Science and Technology, P. O. Box 131, Dong Dae Mun, Seoul 131, Korea *(Received April 23, 1981)*

(1) The flow data of f (stress) and $\dot{s}$ (strain rate) for Fe and Ti alloys were plotted in the form of f *vs.* $-\ln \dot{s}$ by using the literature values. (2) The plot showed two distinct patterns A and B; Pattern A is a straight line with a negative slope, and Pattern B is a curve of concave upward. (3) According to Kim and Ree's generalized theory of plastic deformation, pattern A & B belong to Case 1 and 2, respectively; in Case 1, only one kind of flow units acts in the deformation, and in Case 2, two kinds flow units act, and stress is expressed by $f=X_1f_1+X_2f_2$ where f_1 and f_2 are the stresses acting on the flow units of kind 1 and 2, respectively, and X_1, X_2 are the fractions of the surface area occupied by the two kinds of flow units; $f_j=(1/\alpha_j)\sinh^{-1}\beta_j\dot{s}$ ($j=1$ or 2), where $1/\alpha_j$ and β_j are proportional to the shear modulus and relaxation time, respectively. (4) We found that grain-boundary flow units only act in the deformation of Fe and Ti alloys whereas dislocation flow units do not show any appreciable contribution. (5) The deformations of Fe and Ti alloys belong generally to pattern A (Case 1) and B(Case 2), respectively. (6) By applying the equations, $f=(1/\alpha_{g1})\sinh^{-1}(\beta_{g1}\dot{s})$ and $f=(X_{g1}/\alpha_{g1})\sinh^{-1}(\beta_{g1}\dot{s})+(X_{g2}/\alpha_{g2})\sinh^{-1}(\beta_{g2}\dot{s})$ to the flow data of Fe and Ti alloys, the parametric values of x_{gj}/α_{gj} and β_{gj} ($j=1$ or 2) were determined, here the subscript g signifies a grain-boundary flow unit. (7) From the values of $(\beta_{gj})^{-1}$ at different temperatures, the activation enthalpy ΔH_{gj}^* of deformation due to flow unit gj was determined, $(\beta_{gj})^{-1}$ being proportional to k_{gj}, the jumping frequency (the rate constant) of flow unit gj. The ΔH_{gj}^* agreed very well with ΔH_j^* (self-diff) of the element j whose diffusion in the sample is a critical step for the deformation as proposed by Kim–Ree's theory (Refer to Tables 3 and 4). (8) The fact, $\Delta H_{gj}^*=\Delta H_j^*$ (self-diff), justifies the Kim–Ree theory and their method for determining activation enthalpies for deformation. (9) A linear relation between β^{-1} and carbon content $[C]$ in hot-rolled steel was observed, *i.e.*, $\ln\beta^{-1}=-50.2[C]-40.3$. This equation explains very well the experimental facts observed with regard to the deformation of hot-rolled steel.

1. Introduction

It may be said that the Nabarro–Herring theory[1] of lattice diffusion and Coble's grain boundary diffusion theory[2] are the representatives among many theories of plastic deformation in the literature. The Raj and Ashby equation[3] is an equation which was developed from Nabarro–Herring theory. But, all these theories are applicable in a limited stress region only. Thus, in order to describe plastic deformation in a wide range of stress, a phenomenological equation was proposed.[4] However, it includes many parameters which are lack of physical meanings.

In this study, the Kim–Ree generalized theory of plastic deformation[5–8] is applied to Fe and Ti alloys. This theory is an extension of the Ree–Eyring theory of viscous flow,[9,10] and has an advantage to describe plastic deformation in a wide range of stress, in addition, the physical meanings of the parameter in the equations are clear.

The activation enthalpies ΔH^* for the plastic deformation have been calculated from Kim–Ree's theory, and they have been compared with the activation enthalpies of self-diffusion $\Delta H^*_{\text{self-diff}}$ of the elements in the alloys. It has been found

*Based on the work performed by J. H. Kim in partial fulfilment of the requirement of the degree of Master of Science at the Department of Chemistry, Korea Advaned Institute of Science and Technology, Seoul 131, Korea.

that the ΔH^*'s are in good agreement with $\Delta H^*_{self-diff}$ of elements which play an important role in plastic deformation. This fact accords with the mechanism of plastic deformation proposed by Kim and Ree[5-8] as well as many other authors.[1,2,11] However, the activation enthalpies calculated from classical theories in the literature are generally very different from the $\Delta H^*_{self-diff}$ of the elements, in addition, the values of ΔH^* vary with applied stresses, and are different according to investigators as will be pointed out later.

In this study, the parametric values of the flow equations which were quoted from the Kim-Ree theory have been determined. And, it has been shown that these values are very satisfactory to describe the experimental data of deformation.

These results mentioned above will be reported in this paper, and will be discussed in detail to justify the Kim-Ree thory of plastic deformation.

2. Theory

2.1 Flow Equations

The Ree-Eyring theory[12] treated plastic deformation by using a mechanical model composed of dislocation Maxwell flow units connected in parallel. Hahn, Ree and Eyring[13] incorporated a model which is composed of a dislocation Maxwell flow unit connected in series with a grain-boundary Maxwell flow unit, and explained very successfully the plastic deformation of Yule marble. Kim and Ree[5-8] generalized these theories, and proposed a mechanical model which is composed of a series of dislocation Maxwell flow units connected in parallel and another series of grain-boundary Maxwell flow units which are also connected in parallel, and the two series of flow units are connected in series. From the Kim-Ree model, many cases for plastic deformation are generated by combining various dislocation flow units with various grain-boundary units. In practice, however, four cases are very important, and Kim-Ree's theory was successfully applied by using these four cases.

Among the four cases of the Kim-Ree theory, only Case 1 and Case 2 will be briefly reviewed here since the two cases are important in the present paper. We have also found that in the present case, dislocation flow units do not appear; only the grain-boundary movement will be considered here.

Case 1. In this case, only one kind of grain-boundary flow units is acting. Stress f and strain rate $\dot{s}$ of the flow units are represented by the following equations:

$$f = X_{g1} f_{g1} = \frac{X_{g1}}{\alpha_{g1}} \sinh^{-1} \beta_{g1} \dot{s} \tag{1}$$

and

$$\dot{s} = \frac{1}{\beta_{g1}} \sinh \alpha_{g1} f_{g1} \tag{2}$$

where the subscript $g1$ represents the grain-boundary flow unit of kind 1 on a grain-boundary surface. Thus, f_{g1} expresses the stress acting on flow units $g1$, and X_{g1} shows the fraction of the area occupied by flow units $g1$ on the surface, X_{g1} being unity since there is only one kind ($g1$) of flow units on the surface. Note: $X_{g1}+X_{g2}+\cdots X_{gn}=1$. In Eqs. (1) and (2),

$$\alpha_{g1} = \left(\frac{\lambda\lambda_2\lambda_3}{2kT}\right)_{g1} \tag{3}$$

and

$$\beta_{g1} = \left[\left(\frac{\lambda}{\lambda_1} 2k'\right)_{g1}\right]^{-1} \tag{4}$$

where λ, λ_1, λ_2 and λ_3 are the molecular parameters appearing in Eyring's flow equation,[14] k' is the jumping frequency (rate constant) of a flow unit, and the subscript $g1$ outside parentheses represents the quantity inside parentheses belongs to flow unit $g1$. Speaking of the physical meanings of α_{g1} and β_{g1} the $(\alpha_{g1})^{-1}$ is the intrinsic shear modulus of flow unit $g1$ and β_{g1} the intrinsic relaxation time of flow unit $g1$.

Case 2. In this case, all flow units are connected in parallel. When two kinds of grain-boundary flow units act, the flow equation is represented by the following equations:

$$f = \frac{X_{g1}}{\alpha_{g1}} \sinh^{-1} \beta_{g1}\dot{s} + \frac{X_{g2}}{\alpha_{g2}} \sinh^{-1} \beta_{g2}\dot{s} \tag{5}$$

and

$$\dot{s} = \frac{1}{\beta_{g1}} \sinh \alpha_{g1} f_{g1} = \frac{1}{\beta_{g2}} \sinh \alpha_{g2} f_{g2} \tag{6}$$

where Eqs. (5) and (6) follow from a principle which applies to flow units connected in parallel,[5,6] *i.e.*, $f=\sum_j X_{gj} f_{gj}$ and $\dot{s}=\dot{s}_j$, where $j=1, 2 \ldots n$.

By applying Eqs. (1) and (2) for Case 1 and Eqs. (5) and (6) for Case 2 to experimental flow curves (f *vs.* $\dot{s}$) of the respective cases, the parameters X_{gj}/α_{gj} and β_{gj} (j=1 or 2)are determined. Concerning the method for determining these flow parameters, reference is made to Kim and Ree's paper.[5]

2.2 Calculation of Activation Enthalpies

In Kim and Ree's theory,[5,7,8] the activation enthalpies for plastic deformation is calculated from the following equation:

$$\ln (\beta_{gj})^{-1} = -\frac{\Delta H^*_{gj}}{R} \frac{1}{T} + A_{gj} \tag{7}$$

where, Eq. (7) is derived from Eq. (4), and A_{gj} is a constant. The plot of $\ln (\beta_{gj})^{-1}$ *vs.* $1/T$ according to Eq. (7) yields a straight line whose slope is $-\Delta H^*_{gj}/R$. So,from the slope,the activation enthalpy of the gj flow unit,ΔH^*_{gj},can be obtained.

3. Applications

3.1 Iron Alloys

(*I*) *Fe-1.25Cr-0.45Mo Steel.* Viswanathan[15] examined the creep behavior of Fe-1.25Cr-0.45Mo steel at various temperatures. The composition of this alloys is: Fe(base), Cr(1.3 %), Mo(0.45 %), Mn(0.63 %)., Si(0.45 %), C(0.16 %), and traces of S, N, O, Sb and Sn. By applying Eq. (1) to the flow curves of the Fe alloy, the parameters X_{g1}/α_{g1} (X_{g1}=1) and β_{g1} were determined, and are tabulated in Table 1.

The experimental data[15] of f *vs.* $-\ln \dot{s}$ and the theoretical curves which were calculated from Eq. (1) by using the para-

TABLE 1: Flow Parameters for Several Fe Alloys[a]

Samples	X_{gj}/α_{gj}[b]	$\overset{\circ}{\rho}_{gj}$[b]	Temp. (°C)	Fig.
Fe–1.25Cr–0.45Mo	34.42 (MN/m²)	2.80×10^{5} (hr)	538	Fig. 1
	28.71 (MN/m²)	6.74×10^{4} (hr)	565	
	26.14 (MN/m²)	4.07×10^{4} (hr)	579	
	21.56 (MN/m²)	2.58×10^{4} (hr)	593	
	19.06 (MN/m²)	7.49×10^{3} (hr)	620	
Fe–26Cr–6.5Ni	2.05 (kg/mm²)	2.27×10^{1} (min)	900	Fig. 2
(In 744)	(1.82×10^{-1}) (kg/mm²)	(3.28×10^{4}) (min)		
	1.96 (kg/mm²)	1.06×10^{1} (min)	960	
	(1.67×10^{-1}) (kg/mm²)	(9.69×10^{3}) (min)		
	1.96 (kg/mm²)	6.67 (min)	1020	
	(1.57×10^{-1}) (kg/mm²)	(3.01×10^{3}) (min)		
Type 304	23.75 (Mpa[c])	5.136×10^{9} (sec)	600	Fig. 3
stainless steel	20.50 (Mpa)	8.273×10^{8} (sec)	650	
	17.76 (Mpa)	1.445×10^{8} (sec)	700	
X5CrNiTi26.6	14.53 (N/mm²)	4.48×10^{2} (min)	875	Fig. 4
	13.53 (N/mm²)	1.85×10^{2} (min)	925	
	12.20 (N/mm²)	8.60×10^{1} (min)	975	
Ductile Cast iron	2.23 (kg/mm²)	4.40×10^{3} (min)	650	Fig. 5
M15	1.93 (kg/mm²)	2.13×10^{3} (min)	700	
	1.57 (kg/mm²)	1.26×10^{3} (min)	748	
Ductile cast iron	1.31 (kg/mm²)	1.13×10^{3} (min)	700	Fig. 6
M10	1.22 (kg/mm²)	6.52×10^{3} (min)	748	
	1.12 (kg/mm²)	4.50×10^{3} (min)	780	
Hot-rolled steel				
0.82[d]	1.42×10^{3} (psi)	2.55×10^{35} (sec)	25	Fig. 7
0.70	1.45×10^{3} (psi)	4.28×10^{32} (sec)	25	
0.58	1.44×10^{3} (psi)	1.91×10^{30} (sec)	25	
0.47	1.42×10^{3} (psi)	2.58×10^{28} (sec)	25	
0.32	1.44×10^{3} (psi)	6.26×10^{23} (sec)	25	
0.19	1.41×10^{3} (psi)	3.88×10^{21} (sec)	25	

[a] Unparenthesized parametric values represent the values for flow unit $g1$ and parenthesized ones for flow unit $g2$. [b] Subscript j indicates flow units 1 or 2. [c] MPa=10^6 Pa=10^6 N/m². [d]Carbon content (wt.%).

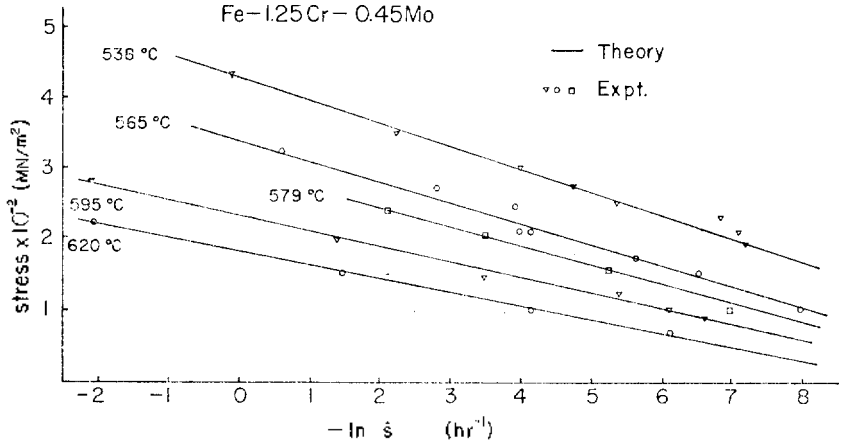

Figure 1. Stress *vs.* −ln ṡ in the creep test of Fe–1.25Cr–0.45Mo steel at temperatures from 538 to 620 °C.

meters in Table 1 are shown in Figure 1. The pattern of the curves in Figure 1 belongs to Case 1 which has only one kind of flow units.

After creep test, Viswanathan[15] observed that fracture occured within the grain in high stress levels, but in low stress levels, the fracture occured at the grain boundary. Here high levels signify the stress above 250 MN/m². By applying Eq. (7) to the experimental curves in Figure 1, the activation enthalpy for deformation was obtained as ΔH_{g1}^{*}=61.4 kcal/g·atom, which is in a good agreement with the activation enthalpy for self-diffusion of Fe. (See Table 3 in the Discussion.) Based on this fact (refer to the Discussion) and on the Viswanathan's fracture observation,[15] we considered that the deformation is caused by the boundary flow units $g1$.

(2) Duplex Stainless Steel (In 744). The composition of commercial In 744 stainless steel is: Fe(base), Cr(26 %) and Ni (6.5 %). Smith *et al.*[16] obtained the relationships of f *vs.* −ln ṡ at three test temperatures. The specimen was flat (width 1 cm, thickness 0.1 cm) and its grain size was about 12 μ after anealing.

The experimental data, obtained by Smith *et al.*,[16] and the theoretical curves, which were calculated from Eq. (5) by using the parameters in Table 1, are shown in Figure 2. The theoretical curves are in good agreement with experimental data. In Figure 2, the pattern of all the flow curves belongs to Case 2 (the parallel connection of GB1 and GB2).

TABLE 2: Flow Parameters for Ti-6Al-4V Alloy[a]

Alloys	X_{gj}/α_{gj}[b] (psi)	α_{gj}[b](sec)	Temp. (°C)	Fig.
Ti-6Al-4V	3.18×10^3	3.32×10^3	800	Fig. 9
	(2.31×10^3)	(8.52×10^4)		
	1.89×10^3	1.89×10^3	900	
	(6.34×10^2)	(1.93×10^4)		
	1.53×10^3	1.56×10^3	950	
	(2.36×10^2)	(9.88×10^3)		
	4.15×10^2	4.72×10^2	990	
	(1.88×10^2)	(2.58×10^5)		
	4.87×10^2	4.55×10^2	1000	
	(1.61×10^2)	(2.33×10^5)		
Ti-5Al-2.5Sn	3.64×10^3	9.57×10^3	700	Fig. 10
	(3.05×10^3)	(3.73×10^5)		
	4.21×10^3	4.95×10^3	750	
	(1.95×10^3)	(2.54×10^5)		
	3.60×10^3	1.64×10^3	800	
	(1.82×10^3)	(1.70×10^5)		
	2.23×10^3	6.28×10^2	900	
	(1.32×10^3)	(9.30×10^4)		
	3.24×10^2	6.50×10^2	1045	
	(1.40×10^2)	(1.79×10^5)		
	$3.00\times10^2)$	6.15×10^2	1055	
	(1.26×10^2)	(1.61×10^5)		
Ti-0.29Si−0.17O_2	1.53 (H bar)	3.29×10^5 (hr)	450	Fig. 11
	1.21 (H bar)	1.20×10^5 (hr)	500	
	0.845 (H bar)	2.37×10^4 (hr)	550	

[a] Unparenthesized parametric values represent the values for flow unit $g1$, and parenthesized ones for flow unit $g2$. [b] The subscript j indicates flow unit 1 or 2.

So, all the flow units are the grain-boundary movement type.

By observation of the microstructure, Smith *et al.*[16] reported that the mechanism of plastic deformation of this alloy is grain boundary sliding in support of our conclusion.

Activation enthalpies, obtained from the flow curves in Figure 2, are shown in Table 3 in the Discussion. The nature of the two kinds of flow units will be made clear later in the Discussion.

(3) *Type* 304 *Stainless Steel.* Chopra *et al.*.[17] studied the creep behavior of Type 304 stainless steel at elevated temperatures. The specimen was a flat sample (length 2.22 cm, width 0.599 cm, thickness 0.038 or 0.127 cm) and its grain size was about 25μ. The composition of this alloy was: Fe (base), Cr (18 to 20 %), Ni (8 to 10.5 %), Mn (max 2 %), traces of Si, C, S and P.

The experimental data[17] of f *vs.* $-\ln\dot{s}$ are plotted in Figure 3. The parameters for the flow curves of this alloy are given in Table 1, from which the theoretical curves were calculated from Eq. (1), and are shown in Figure 3. The latter shows that the pattern of the flow curves belongs to Case 1.

Chopra *et al.*[17] observed that the grains did not change measurably in the length-to-width ratio within the overall deformation range of the specimen. From this observation, the flow mechanism is expected to be grain boundary movement.

The activation enthalpies for deformation, obtained from the slope of the plot of $\ln\beta^{-1}$ *vs.* $1/T$, are shown in Table 3 in the Discussion.

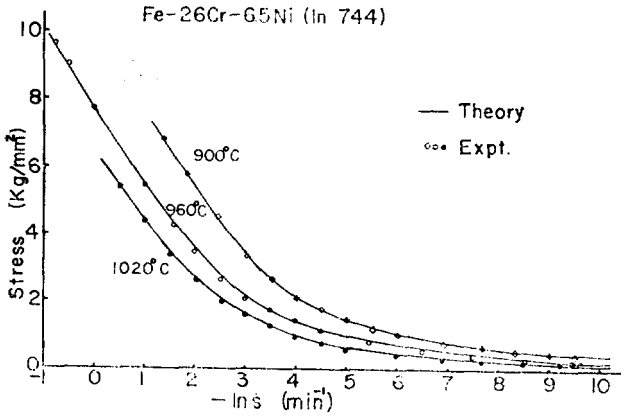

Figure 2. Stress *vs.* -ln ṡ for Fe-26Cr-6.5Ni (*In* 744) alloy at 900, 960 and 1020 °C.

(4) *Steel X5CrNiTi26.6.* Hildebrand *et al.*.[18] studied the plastic deformation of steel X5CrNiTi26.6 the composition of which is: Fe(base), Cr(25.5 %), Ni(6.28 %), Mn(0.68 %), Ti(0.32 %), traces of Si, P, S, Al, Cu and N.

The experimental data[18] of tensile test for these specimens are plotted in Figure 4, and theoretical curves which were obtained by introducing the flow parameters (Table 1) into Eq. (1) are also shown in Figure 4.

In Figure 4, all the flow curves belong to Case 1, *i.e.*, only one kind of flow units is acting. It is expected that the type of flow units in this case would be a grain boundary movement type, because, according to microstructural observa-

TABLE 3: ΔH_{gj}^{*} Values for Fe Alloys[a]

Samples	ΔH_{gj}^{*} (kcal/g·atom)	Range of temp.(°C)	Ref.
Fe-1.25Cr-0.45Mo	61.4 [ΔH_{g1}^{*} (Fe)]	538–620	This work
Fe-26Cr-6.5Ni	31.4 [ΔH_{g1}^{*} ( )]	900–1020	This work
(In 744)	60.4 [ΔH_{g2}^{*} (Fe)]		
Type 304 stainless steel	60.2 [ΔH_{g1}^{*} (Fe)]	600–700	This work
X5Cr NiTi26.6	47.1 [ΔH_{g1}^{*} (Cr)]	875–975	This work
^{55}Fe in γ-iron	$\Delta H^{*}_{self-diff}$: 64.0	900–1200	Boksztein *et al.*[23]
^{55}Fe in α-iron	$\Delta H^{*}_{self-diff}$: 60.0	700–790	Buffington *et al.*[24]
^{55}Fe in α-iron	$\Delta H^{*}_{self-diff}$: 60.7	638–768	James *et al.*[25]
^{51}Cr in Fe-26.0Cr	$\Delta H^{*}_{self-diff}$: 48.5	950–1275	Paxton *et al.*[26]
Ductile cast iron M15	24.1 [ΔH_{g1}^{*} (C)]	650–748	This work
Ductile cast iron M10	23.5 [ΔH_{g1}^{*} (C)]	700–780	This work
^{14}C in α-iron	ΔH^{*}_{diff}: 24.6	500–800	Gruzin *et al.*[27]

[a] ΔH_{g1}^{*} and ΔH_{g2}^{*} represent activation enthalpies for flow units $g1$ and $g2$, respectively. The expected diffusing atoms are given in parentheses.

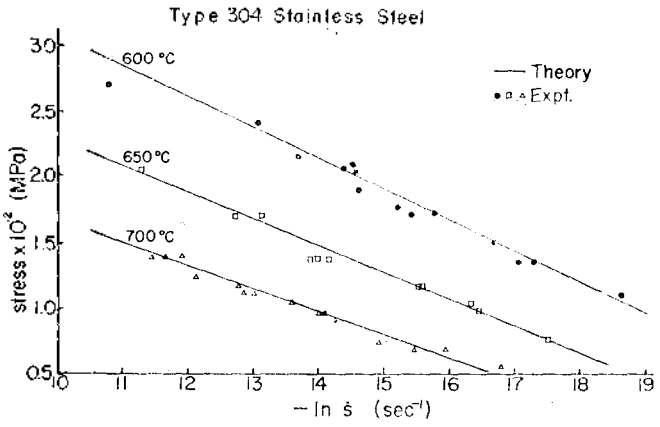

Figure 3. Stress *vs.* −ln ṡ in the creep test of type 304 stainless steel at 600, 650 and 700 °C.

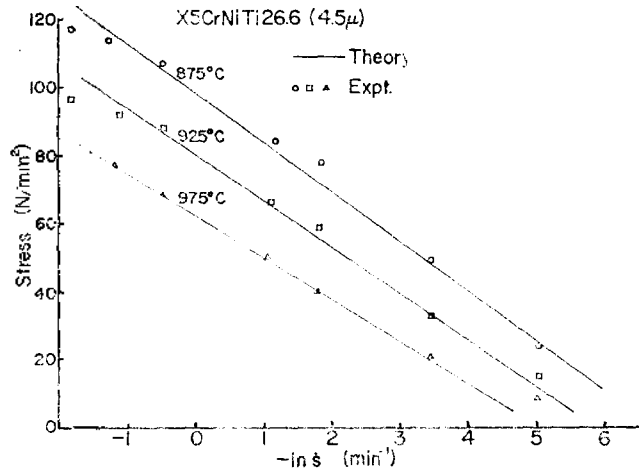

Figure 4. Stress *vs.* −ln ṡ for X5CrNiTi26.6 steel at 857, 925 and 975 °C.

tion[18] of Hildebrand *et al.*, the microstructure of specimens did not change significantly after tensile test.

The activation enthalpy, obtained from the flow curves, are shown in a later table (Table 3).

(5) *Ductile Cast Iron.* Tanaka *et al.*[19] studied the tensile deformation of ductile cast irons which are named as M15 and M10. The specimens were cylinders (diameter 5 mm, length 25 mm) with a very fine microstructure. The composition of the M15 alloy is: Fe (base), C(3.2 %), Si (1.95 %) and Mn (1.42 %), and that of the M10 alloy is: Fe(base), C(3.08 %), Si(1.84%) and Mn(0.92%), each alloy having traces of P, S and Mg.

Experimental data of f *vs.* −ln ṡ for M15 and M10 are shown in Figures 5 and 6, respectively. The flow curves show that they belong to Case 1, *i.e.*, only one kind of flow units acts in the deformation. In Figures 5 and 6, the solid lines are theoretical curves calculated by introducing the flow parameters in Table 1 into Eq. (1).

According to microscopic observations of Tanaka *et al.*[19] the grain size of M10 after tensile test increased very little, and that of M15 remained the same. Thus the flow unit for deformation of these alloy is considered to be a grain boundary movement type.

Activation enthalpies calculated from the experimental data are shown in Table 3 in the Discussion.

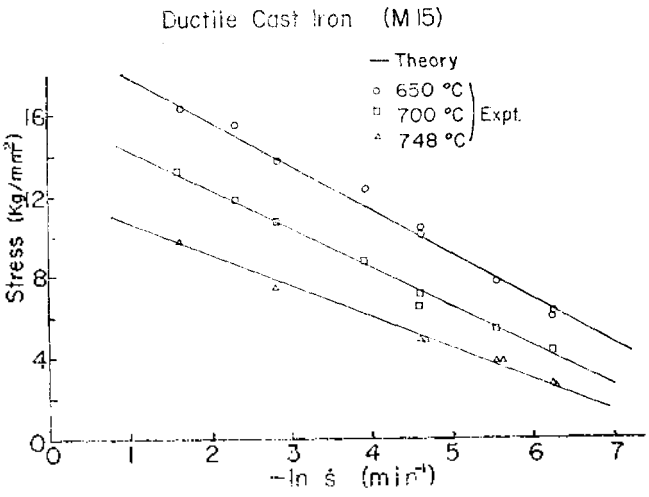

Figure 5. Stress *vs.* −ln ṡ for ductile cast iron (M15) at 650, 700 and 748 °C. The phase of M15 is $\alpha+\beta+$cementite.

(6) *Carbon Content Dependence of β in Hot-Rolled Steel.* Davis *et al.*[20] studied the tensile deformation of hot-rolled steel at room temperature, the composition of the specimen being: Fe(base), Mn(average 0.75 %) and carbon (varied from 0.19 to 0.82 %, Figure 7).

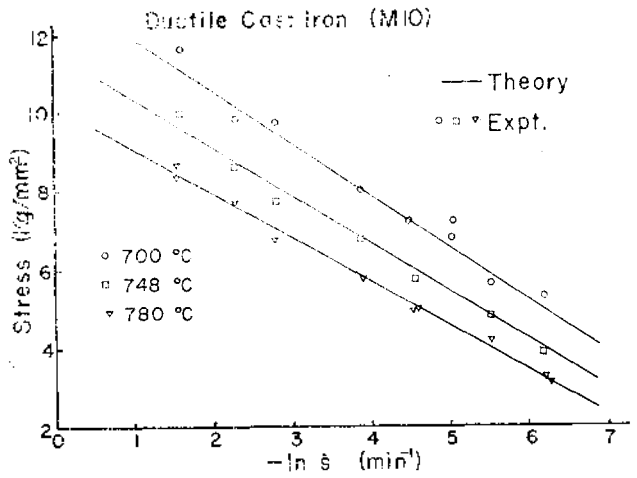

Figure 6. Stress *vs.* −ln ṡ for ductile cast iron (M10) at 700, 748 and 780 °C. The phase of M10 is γ+cementite.

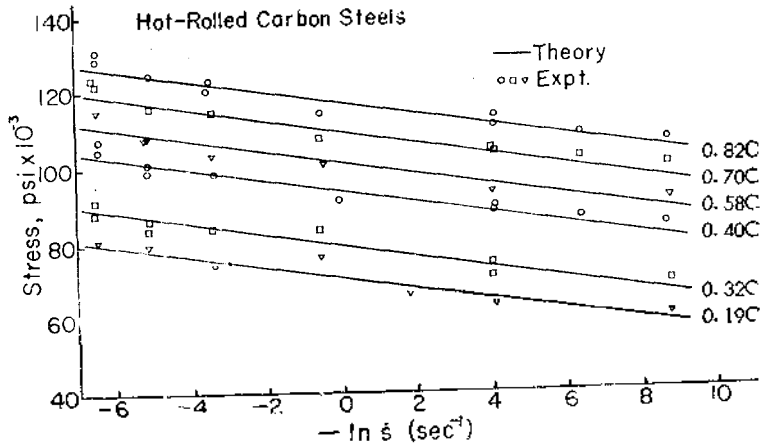

Figure 7. Stress *vs.* −ln ṡ for hot-rolled carbon steel with carbon contents varying from 0.19 to 0.82 weight percent at 25 °C.

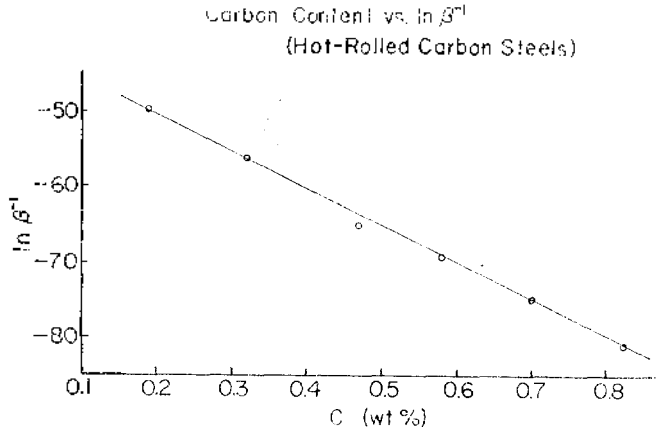

Figure 8. ln β^{-1} *vs.* carbon contents in the hot-rolled carbon steel. The quantity β^{-1} is proportional to jumping frequency (rate constant) of a flow unit.

The theoretical curves of f *vs.* −ln ṡ which were calculated by introducing the parameters in Table 1 into Eq. (1) are compared with the experimental data[20] in Figure 7. And the relationship of ln β^{-1} *vs.* carbon content [C] are plotted in Figure 8.

In Figure 8, the plot of ln β^{-1} *vs.* [C] yields a straight line. Its slope and intercept are determined by a least square method. Thus, the straight line is expressed by

$$\ln \beta^{-1} = -50.2[C] - 40.3 \quad (8)$$

where [C] is in units of weight percentage of C, and β in sec^{-1}.

According to Eq. (8), β increases rapidly with [C]. Thus, in accordance with Eq. (1), the deformation of high [C] steel requires higher stress than low [C] steel at any constant ṡ as shown in Figure 7.

3.2. Titanium Alloys

(1) *Ti-6Al-4V Alloy.* Lee *et al.*[21] studied the tensile deformation of Ti-6Al-4V alloy [Ti(base), Al(6 %), V(4 %)] at various temperatures. The experimental data[21] of f *vs.* −ln ṡ and theoretical curves calculated from Eq. (5) by/ṡ using the parameters in Table 2 are shown in Figure 9./m In the inset of Figure 9, are shown the flow curves at 800 to 950 °C when the sample exists as an α phase. At 990 and 1000 °C, the phase is changed to β while it is a mixed $\alpha+\beta$ phase at 980 °C. The experimental flow curves for these phases are also shown in Figure 9. All the flow curves belong to Case 2 in which two types of grain boundary flow units appear.

The microstructural observation[21] of the specimen showed that no change in grain size occured before and after tensile deformation. This fact accord with our assumption that the type of flow units belong to grain boundary movement.

One notes from Figure 9 that the flow curve at 980 °C for the $\alpha+\beta$ phase shows a breaking point at $-\ln \dot{s} \simeq 8$. It is not clear at present whether this fact caused by the change of structure due to applied stress or not.

The activation enthalpies of deformation in α and β phases were calculated by Kim and Ree's theory, and are shown in Table 4 in the Discussion.

(2) *Ti-5Al-2.5Sn Alloy.* Lee *et al.*[21] examined the tensile deformation of Ti-5Al-2.5Sn alloy with the same method as in Ti-6Al-4V alloy. The specimen was made of a commercial Ti-5Al-2.5Sn alloy, the composition is: Ti(base), Al(5 %) and Sn(2.5 %).

The experimental data of f *vs.* −ln ṡ and the theoretical curves for this alloy calculated from Eq. (5) by using the parameters in Table 2 and shown in Figure 10. All the flow curves show the flow character of Case 2. In the inset of Figure 10, the flow curves at 700 to 900 °C are shown where the phase of the sample is α. It changes the phase at higher temperatures, *i.e.*, it is β at 1045 and 1055 °C while it is a mixed $\alpha+\beta$ phase at 1022 and 1030 °C. The flow curves at the higher temperatures are also shown in Figure 10.

The microstructural observations[21] of the samples in Figure 10 showed that the grain size increased affter tensile test. The size increase may occur by combination of grains which moved together by grain boundary movement. Thus the

TABLE 4: ΔH_{α}^{*} Values for Ti Alloys[a]

Alloys	ΔH_{α}^{*} (kcal/g·atom)	Phase	Ref.
Ti-6Al-4V	11.9 [$\Delta H_{\beta 1}^{*}$ (Al)]	β	This work
	33.3 [$\Delta H_{\beta 2}^{*}$ (Ti)]		
	10.6 [$\Delta H_{\alpha 1}^{*}$ (Al)]	α	This work
	31.7 [$\Delta H_{\alpha 2}^{*}$ (Ti)]		
Ti-5Al-2.5Sn	19.3 [$\Delta H_{\beta 1}^{*}$ (Sn)]	β	This work
	36.3 [$\Delta H_{\beta 2}^{*}$ (Ti)]		
	15.6 [$\Delta H_{\alpha 1}^{*}$ (Sn)]	α	This work
	31.9 [$\Delta H_{\alpha 2}^{*}$ (Ti)]		
Ti-0.29Si-0.17O_2	31.0 [$\Delta H_{\beta 1}^{*}$ (Ti)]	α	This work
Self-diffusion of Ti^{44} in Ti	$\Delta H_{\text{self-diff}}^{*}$		
	31.2 kcal/g·atom	β	Murdock *et al.*[28]
Self-diffusion of Ti^{44} in Ti	$\Delta H_{\text{self-diff}}^{*}$		
	29.3 kcal/g·atom	α	Libanati *et al.*[29]

[a] $\Delta H_{\beta 1}^{*}$ and $\Delta H_{\beta 2}^{*}$ represent activation enthalpies for flow units g_1 and g_2, respectively. The expected diffusing atoms are given in parentheses.

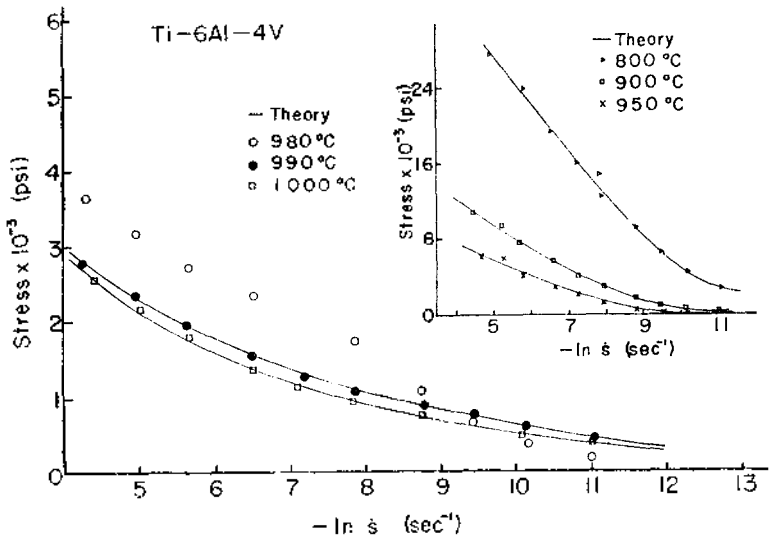

Fig. 9. Stress *vs.* −ln ṡ for Ti-6Al-4V alloy. The flow curves at 800 to 950 °C, where the phase of the sample is α, are given in the inset figure. The phase is β at 990 and 1000 °C, and it is $\alpha+\beta$ at 980 °C.

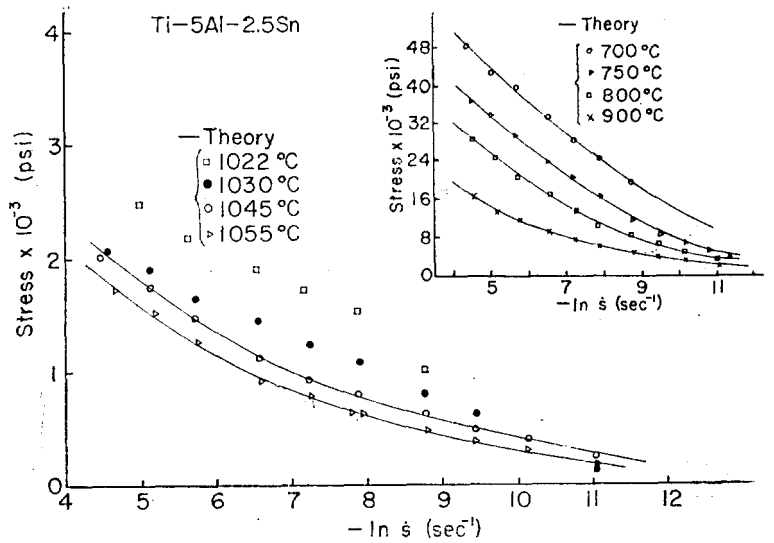

Fig. 10. Stress *vs.* −ln ṡ for Ti-5Al-2.5Sn alloy. The flow curves at 700 to 900 °C, where the phase of the sample is α, are given in the inset figure. The phase is β at 1045 and 1055 °C, and it is $\alpha+\beta$ at 1022 and 1030 °C.

grain size increase seems to surpport our assumption that the grain-boundary movement controlled the deformation of the alloy.

One notes from Figure 10 that the flow curves at 1022 and 1030 °C(where the phase is $\alpha+\beta$) show the same phenomenon observed for the phase of $\alpha+\beta$ of Ti-6Al-4V alloy in Figure 9, *i.e.*, the Ti-5Al-2.5Sn alloy shows also a breaking point at $\simeq -\ln \dot{s}=8$. The reason for it is not clear at present, but it may be said that this phenomenon is a common character for a sample of mixed phase.

The activation enthalpies of deformation in α and β phase are calculated by our method, and are shown in Table 4 in the Discussion.

(3) *Ti-0.29Si-0.17O_2.* Kohoe *et al.*[22] studied the creep deformation of Ti-0.29Si-0.17O_2 alloy at three test temperatures (450, 500, 550 °C) where the phase of the sample is α. The experimental data and theoretical curves, calculated from Eq. (5) by using the parameters in Table 2 are shown in Figure 11. Each flow curve belongs to Case I which is due to only one kind of flow units. Since this alloy contains very small contents of Si and O_2, the only one kind of flow units mentioned above is considered to be Ti.

Kohoe *et al.*[22] observed optically the microstructure of the sample before creep test, and found that very large grains exist, and also by an electron microscopic examination, they observed many fine and parallel boundaries within the large grains. After creep test, however, the microsructure was not changed, and there was almost no precipitation; these phenomena show that this alloy is considerably stable for defor-

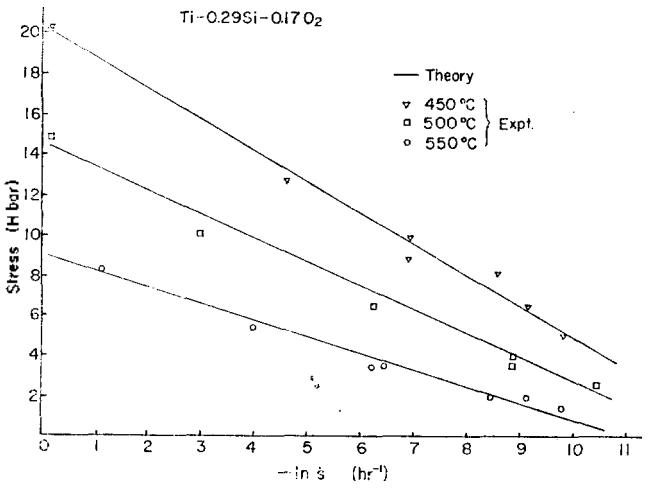

Figure 11. Stress *vs* $-\ln \dot{s}$ for the creep test of Ti–0.29Si–0. $17O_2$ alloy at 450, 500 and 550 °C. At these temperatures, the phase of the sample is α.

mation. From these observations, it may be said that the mechanism of deformation is a grain boundary movement which occurs on the fine boundaries in the large grains.

The activation enthalpy calculated by using the parameters in Table 2 is shown in Table 4 in the Discussion.

4. Discussion

1. *Activation Enthalpiesfor Grain Boundary Flow of Fe Alloys.*

According to the Kim-Ree theory of plastic deformation,[5–8] the movement of a flow unit is hindered by an element in the sample, thus diffusing of the element away from the spot of hindrance is a necessary condition for continuing the movement of the flow unit, *i.e.*, for the deformation. From this view point, Kim and Ree concluded that the activation enthalpy for plastic deformation is equal to that for self-diffusion $\Delta H^*_{self-diff}$ of the critical element. Therefore, in this study, the activation enthalpies for plastic deformation of Fe and Ti alloys were calculated from Eq. (7), and compared with $\Delta H^*_{self-diff}$ of the elements which are considered to be critical in the flow process.

First, consider the case of Fe–1.25Cr–0.45Mo alloy (Figure 1). The activation enthalpy for the deformation of the alloy is found to be ΔH^*_{g1}=61.4 kcal/g·atom by our method. The activation enthalpy of self-diffusion of Fe is about 60 kcal/g·atom[23–25] as shown in Table 3. (See the terms of $\Delta H^*_{self-diff}$ in the column of ΔH^*_{gi}). Therefore, our value ΔH^*_{g1}=61.4 kcal/g·atom is in good agreement with $\Delta H^*_{self-diff}$ of Fe as predicted by the Kim-Ree theory. By using classical method, however, Viswanathan[15] obtained 76.2 kcal/g·atom as the activation enthalpy for the deformation, but it is quite different from $\Delta H^*_{self-diff}$ of Fe.

Next consider the case for Fe–26Cr–6.5Ni alloy (In 744) (Figure 2) which was studied by Smith *et al.*[16] The two kinds of activation enthalpies (ΔH^*_{g1} and ΔH^*_{g2}) were calculated by our method, and are shown in Table 3. The value ΔH^*_{g1} =31.4 kcal/g·atom will be considered later. But, the value ΔH^*_{g2}=60.4 kcal/g·atom (Table 3) is in good agreement with $\Delta H^*_{self-diff}$ of Fe.[23–25] (Refer to Table 3.) Thus the value of ΔH^*_{g2} is considered due to the self-diffusion of Fe atoms.

For the case of Type 304 stainless steel[17] (Figure 3), the value ΔH^*_{g1}=60.2 kcal/g·atom was obtained by our method, and it is also in good agreement with. $\Delta H^*_{self-diff}$ of Fe.[23–25] Chopra *et al.*[17] reported that the apparent activation enthalpy decreased from 91.7 to 79.5 kcal/g·atom when the stress decreases from high to low stresses. But these values are unreliable since they are different from $\Delta H^*_{self-diff}$ of Fe, and the value of activation enthalpy changes with stress.

The activation enthalpy for deformation of steel X5Cr NiTi-26.6 (Figure 4) was calculated as ΔH^*_{g1}=47.1 kcal/g· atom by our method, and it is in good agreement with 48.5 kcal/g·atom which is $\Delta H^*_{self-diff}$ of ^{51}Cr in Fe–26Cr alloy.[26] (Refer to Table 3.) Therefore, the creep deformation of steel X5CrNiTi26.6 in the tested stress region is considered to be mainly controlled by Cr than the base metal Fe.

Next,we consider the value of ΔH^*_{g1}=31.4 kcal/g·atom for In 744 (Figure 2). In the determination of this value, we used the values of β_{g1} at 900, 960 and 1020 °C. (See Figure 2 and refer to Eq. 7.) Except at 960 °C, the experimental flow data for the curves at 900 and 1020 °C are very scanty for determining β_{g1} which appear in the range of $-\ln \dot{s}=-1$ to 3, *i.e.*, only three and four data are available at 900 and 1020 °C, respectively. (Refer to Figure 2.) Consequently, the accuracy of β_{g1} values at these temperatures is not so good. Since ΔH^*_{g1} is obtained by using the values of β_{g1} at 900, 960 and 1020°C, we believe that the value of ΔH^*_{g1}=31.4 kcal/g-atom is underestimated more than by 10 kcal. If this is the case, the $g1$ unit is controlled by the diffusion of Cr. For definite understanding of flow unit $g1$, however, more accurate flow daa are required for the sample, In 744.

In the case of ductile cast irons M15 and M10 (Figures 5 and 6),[19] the activation enthalpies are about ΔH^*_{g1}=24 kcal/g·atom (Table 3) for both alloys. This value is in good agreement with $\Delta H^*_{self-diff}$ of ^{14}C in α-Fe.[27] (See Table 3.) M15 and M10 alloys contain relatively large amount of carbon, *i.e.*, 3. 20 and 3.08 %, respectively, but, the Mn content is relatively samall, *i.e.*, 1.42 % and 0.92 %, respectively. From the above-mentioned facts, it may be concluded that the flow unit of deformation is related to carbon, but not by the base metal Fe or Mn.

Tanaka *et al.*[19] reported that Mn has an action stabilizing the carbide in cast iron. According to our study, however, it is found that carbon, but not Mn, is related to flow of the sample in the test stress region.

The phase of M15 is $\alpha+\gamma+$cementite and that of M10 is $\gamma+$cementite. Though the phases are different from each other, the activation enthalpies of deformation for the two alloys are similar, about 24 kcal/g·atom. From this result, if the composition of alloys are similar, it is expected that the

activation enthalpies of deformation are about equal inspite of the phase difference.

2. *Activation Enthalpies for Grain Boundary Flow of Ti Alloys.*

The activation enthalpies for deformation of Ti–6Al–4V alloy (Figure 9) are shown in Table 4. The phase of this alloy is β at temperatures above 990 °C. In this phase, the activation enthalpy for flow unit $g1$ is $\Delta H_{g1}^{*}=11.9$ kcal/g·atom, which is in a good agreement with $\Delta H_{\text{self-diff}}^{*}$ of Al which is reported in the Kim–Ree theory.[7,8] The activation enthalpy for flow unit $g2$ is $\Delta H_{g2}^{*}=33.3$ kcal/g·atom, which agrees with those values of $\Delta H_{\text{self diff}}^{*}$ of Ti (about 30 kcal/g·atom).[28,29] (Refer to the lowest part of Table 4.)

For the α–phase of Ti–6Al–4V alloy (Figure 9), the activation enthalpies for flow units g1 and g2 are found to be $\Delta H_{g1}^{*}=10.6$ and $\Delta H_{g2}^{*}=31.7$ kcal/g·atom, respectively, and these values are similar with those for β–phase ($\Delta H_{g1}^{*}=11.9$, $\Delta H_{g2}^{*}=33.3$ kcal/g·atom), and these values are also in good agreement with $\Delta H_{\text{self-diff}}^{*}$ of Al[7,8] and Ti,[28,29] respectively.

For Ti–5Al–2.5Sn alloy (Figure 10), the activation enthalpy for flow unit $g1$ is calculated as $\Delta H_{g1}^{*}=19.3$kcal/g·atom for β–phase (flow curves at 1045 and 1055 °C) and as $\Delta H_{g1}^{*}=15.6$kcal/g·atom for α–phase(the inset curves). (Refer to Table 4 and Figure 10.) These values deviate a little from 22.4 kcal/g·atom which is $\Delta H_{\text{self-diff}}^{*}$ of Sn[30] at 130 to 250° C. But, this temperature range is far below than 700 to 1055 °C where we obtained ΔH_{g1}^{*} for the deformation. Thus, the small difference in ΔH_{g1}^{*} and $\Delta H_{\text{self-diff}}^{*}$ of Sn is expected to be natural.

The activation enthalpy for flow unit $g2$ of Ti–5Al–2.5Sn alloy is $\Delta H_{g2}^{*}=36.3$ kcal/g·atom in β–phase and $\Delta H_{g1}^{*}=31.9$ kcal/g·atom in α–phase (Table 4), and these values agree with $\Delta H_{\text{self-diff}}^{*}$ of Ti,[28,29] about 30 kcal/g·atom (Table 4).

Lee *et al.*[21] reported the activation enthalpy for Ti–5Al–2.5Sn alloy as 50 to 65 kcal/g·atom which was obtained by classical method, and this value changed according to stress levels. This value is about twice of $\Delta H_{\text{self-diff}}^{*}$ of Ti. Thus, Lee *et al.*'s value for activation enthalpy is considered to be unreliable.

The Ti–0.29Si–0.17O_2 alloy (Figure 11) is nearly pure titanium. Thus we obtained only one kind of flow units. The activation enthalpy for this flow unit is found to be $\Delta H_{g1}^{*}=31.0$ kcal/g·atom by our method (Table 4), and it is in good agreement with $\Delta H_{\text{self diff}}^{*}$ of Ti (about 30 kcal/g·atom). (Refer to Table 4.)

Kohoe *et al.*[22] calculated the apparent activation enthalpy by a classical method as 68 to 72 kcal/g·atom, but this value is also more than twice of $\Delta H_{\text{self-diff}}^{*}$ of Ti. Thus, we believe Kohoe *et al.*'s value is not reasonable.

From the above results, the values of ΔH_{g1}^{*} obtained by our method is more reliable than the values obtained by classical method reported in the literature.

Acknowledgment. Our grateful acknowledgment is due to the support of this work by the Korea Research Center for Theoretical Physics and Chemistry.

References

(1) C. Herring, *J. Appl. Phys.*, **21**, 437 (1950).
(2) R. L. Coble, *J. Appl. Phys.*, **34**, 1679 (1963).
(3) R. Raj and M. F. Ashby, *Met. Trans.*, **2**, 1113 (1971).
(4) F. A. Mohamed and T. G. Langdon, *Phil. Mag.*, **32**, 697 (1977).
(5) C. H. Kim and T. Ree, *J. Korean Chem. Soc.*, **21**, 330 (1977).
(6) C. H. Kim and T. Ree, J. Korean Chem. Soc., **21**, 339 (1977).
(7) C. H. Kim and T. Ree, *J. Korean Chem. Soc.*, **23**, 217 (1979).
(8) C. H. Kim and T. Ree, *Bull. Korean Chem. Soc.*, **1**, 39 (1980)..
(9) T. Ree and H. Eyring, *J. Appl. Phys.*, **26**, 793 (1955).
(10) T. Ree and H. Eyring, *J. Appl. Phys.*, **26**, 800 (1955).
(11) S. W. Zehr and W. A. Backofen, *Trans. Quart. A.S.M.*, **61**, 300 (1968).
(12) F. H. Ree, T. Ree and H. Eyring, *Am. Soc. Civil Engineers Trans.*, **128**, 1321 (1963).
(13) S. J. Hahn, T. Ree and H. Eyring, *Geol. Sco. Am. Bull.*, **78**, 773 (1967).
(14) H. Eyring, *J. Chem. Phys.*, **4**, 283 (1936).
(15) R. Viswanathan, *Met. Trans.*, **8A**, 877 (1977).
(16) C. I. Smith, B. Norgate and B. Ridley, *Scrip. Met.*, **8**, 159 (1974).
(17) O. K. Chopra and K. Natesan, *Met. Trans.*, **8A**, 633(1977).
(18) H. Hildebrand, G. Michalzik and B. Simmen, *Met. Tech.*, 32 (1977).
(19) Y. Tanaka and K. Ikawa, *J. Japan Inst. Metals.* **38**(9), 865 (1974).
(20) R. G. Davies and C. L. Magee, *J. Eng. Mat. Tech.*, 151 (1975).
(21) D. Lee and W. A. Backofen, *Trans. Metall. Soc. AIME.*, **239**, 1034 (1967).
(22) J. Kehoe and R. W. Broomfield, "Titanium Science and Technology", Ed. R. I. Jaffee and H. M. Brute, p. 2167–2178, Plenum press, New York, 1973.
(23) S. Z. Bokshtein, S. T. Kishkin and L. M. Moroz, "Tracer Diffusion Data for Metals, Alloys and Simple Oxides," Ed. J. Askill, p. 34, IFI/Plenum Data Cooperation, New York, 1970.
(24) F. S. Buffington, K. Hirano and M. Cohen, *Acta Met.*, **9**, 434 (1961).
(25) D. W. James and G. M. Leak, *Phil. Mag.*, **14**, 701 (1966).
(26) H. W. Paxton and T. Kunitake, *Trans. Metall. Soc. AIME.*, **218**, 1003 (1960).
(27) P. L. Gruzin and D. F. Litvin, "Tracer Diffusion Data for Metals, Alloys and Simple Oxides," Ed. J. Askill, p.46, IFI/Plenum Data Cooperation, New York, 1970.
(28) J. F. Murdock, T. S. Lundy and E. E. Stansbury, *Acta Met.*, **12**, 1033 (1964).
(29) C. M. Libanati and S. F. Dyment, *Acta Met.*, **11**, 1263 (1963).
(30) W. Lange and A. Hassner, *Phys. Stat. Sol.*, **1**, 50 (1961).